Hippocampal–cortical coupling differentiates long-term memory processes

Prawesh Dahal[a,b,1], Onni J. Rauhala[a,b,1], Dion Khodagholy[a,2] (ID), and Jennifer N. Gelinas[b,c,2]

Reactivation of long-term memories enables experience-dependent strengthening, weakening, or updating of memory traces. Although coupling of hippocampal and cortical activity patterns facilitates initial memory consolidation, whether and how these patterns are involved in postreactivation memory processes are not known. Here, we monitored the hippocampal–cortical network as rats repetitively learned and retrieved spatial and nonspatial memories. We show that interactions between hippocampal sharp wave–ripples (SPW-R), cortical spindles (SPI), and cortical ripples (CXR) are jointly modulated in the absence of memory demand but independently recruited depending on the stage of memory and task type. Reconsolidation of memory after retrieval is associated with an increased and extended window of coupling between hippocampal SPW-Rs and CXRs compared to the initial consolidation. Hippocampal SPW-R and cortical spindle interactions are preferentially engaged during memory consolidation. These findings suggest that specific, time-limited patterns of oscillatory coupling can support the distinct memory processes required to flexibly manage long-term memories in a dynamic environment.

consolidation | hippocampus | learning | memory | ripples

Newly formed memories become more stable and durable through memory consolidation (1). Retrieval of a consolidated memory can reopen a window of lability, after which the memory can be strengthened, updated, or weakened depending on the nature of the retrieval experience (2). Memory restabilization involves a process termed reconsolidation, which recruits brain regions and certain signaling pathways that are distinct from those involved in the initial consolidation (3, 4). Naturalistic behaviors strongly hinge on this flexible modulation of long-term memory because the salience of environmental stimuli frequently changes (5). Yet, how neural activity patterns support memory across these dynamic phases remains unexplored.

Interactions between medial temporal lobe structures, especially the hippocampus, and cortical regions are critical for long-term memory (6). Rapid encoding of an episode is postulated to occur in the hippocampus, with subsequent functional maturation of cortically based memory that requires hippocampal input (7–9). In keeping with this notion, targeted and reversible inactivation of cortical areas can result in impairment of retrieval of remote but not recent memory (10–13). Such interactions are best delineated for tasks that involve spatial information, but the hippocampus is also implicated in consolidation of nonspatial tasks (14, 15).

During nonrapid eye movement (NREM) sleep, behaviorally relevant neural activity patterns are reinstated in the hippocampus and cortex. Temporal coordination between these structures provides a substrate for interregional communication (16–21). Hippocampal and cortical oscillations including hippocampal sharp wave–ripples (SPW-R), cortical sleep spindles (SPI), and cortical ripples (CXR) are postulated to facilitate such interactions. SPW-R are required for memory (22, 23), and enhancing their pairing with cortical spindles converts a subthreshold experience to one sufficient for induction of long-term memory (24). CXR are temporally coupled to SPW-R in a learning-dependent manner (25), and this temporal association is engaged during successful memory retrieval (26).

These patterns of hippocampal–cortical communication have been independently identified and characterized during consolidation, but their role outside of this initial memory processing epoch is unknown. We hypothesized that these oscillatory coupling patterns would be i) jointly modulated in response to memory demand and ii) differentially recruited after a consolidated memory was retrieved. To test this hypothesis, we monitored hippocampal–cortical network activity as rats performed cycles of spatial and nonspatial long-term memory tasks that required repeated consolidation, reconsolidation, and updating within a consistent behavioral schema. We found that although interactions between SPW-R, SPI, and CXR are tightly linked in the absence of memory demand, they are

Significance

Long-term memories are dynamic, but the network patterns that enable this behavioral flexibility are not well understood. In the present study, we show that activity in the hippocampus and cortex is differentially coordinated based on the age, strength, and type of memory. Our findings may be useful in identifying markers of different ongoing memory processes and understanding mechanisms that lead to both impaired and overactive information retention.

Author affiliations: [a]Department of Electrical Engineering, Columbia University, New York, NY 10027; [b]Institute for Genomic Medicine, Columbia University Medical Center, New York, NY 10032; and [c]Department of Neurology, Columbia University Medical Center, New York, NY 10032

[1]P.D. and O.J.R. contributed equally to this work.

[2]To whom correspondence may be addressed. Email: dk2955@columbia.edu or jng2146@cumc.columbia.edu.

independently recruited depending on the nature of the task and the stage of memory processing. Consolidation and reconsolidation were differentiable based on the predominant pattern of hippocampal–cortical coupling and its temporal dynamics across NREM sleep. The precise, time-limited tuning of SPW-R, SPI, and CXR interactions after different memory-related experiences provides a possible substrate for the flexible processing of long-term memory in a dynamic environment.

Results

We used a conducting polymer-based conformable microelectrode surface array (NeuroGrid) in tandem with implanted probes to perform concomitant electrophysiological monitoring of the cortex and hippocampus in behaving rats (n = 9 rats). We targeted signals derived from the posterior parietal cortex (PPC) due to its known interaction with the hippocampus, functional participation in distributed networks involved in formation and retrieval of episodic memory, and its ability to form an enduring cortical engram shortly after learning (27–30).

To identify NeuroGrid electrodes recording from the PPC, we combined electrophysiological and anatomical markers (Fig. 1*A* and *SI Appendix*, Fig. S1). We first explored the occurrence of hippocampal and PPC activity patterns during NREM sleep in the absence of a structured task. Hippocampal traces exhibited characteristic SPW-R, and we detected cortical slow oscillations, SPI, and CXR from PPC traces (Fig. 1*B*). These oscillatory patterns occurred at expected rates, and detection parameters were optimized for sensitivity and specificity (*SI Appendix*, Figs. S1 and S2, *Materials and Methods*). SPW-R and cortical oscillations have significant temporal coupling (25, 31–33) (Fig. 1*C*), and we aimed to investigate how these coupling dynamics are coordinated. SPW-R and CXR were strongly and precisely coupled compared to a more modest coupling between SPW-R and SPI (Fig. 1*D*).
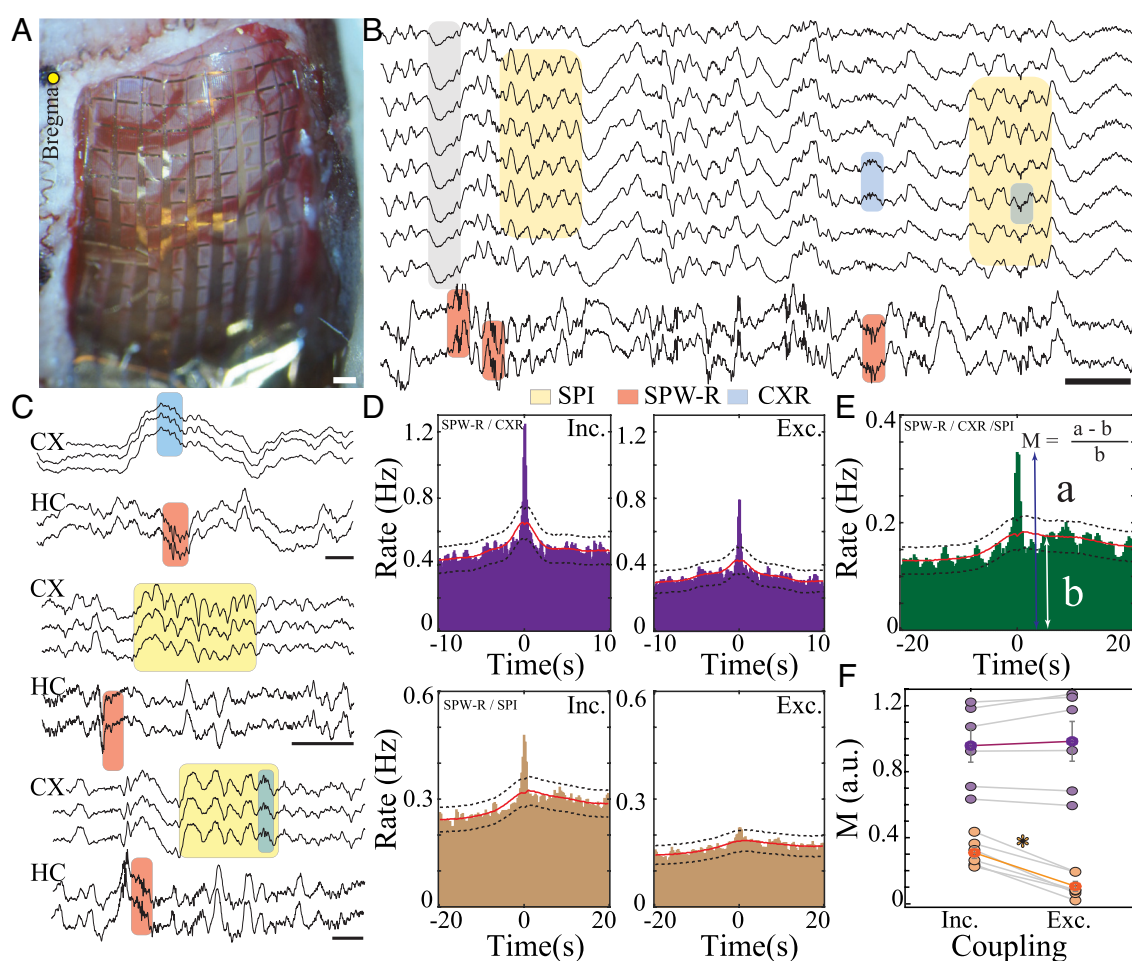

Fig. 1. Hippocampal–cortical interactions are jointly modulated in the absence of memory demand. (*A*) NeuroGrid array conforming over the dorsal cortical surface of a rat from bregma (yellow dot) anteriorly to lambda posteriorly. (Scale bar, 1 mm.) (*B*) Sample wide-band LFP traces (0.1 to 1,250 Hz) simultaneously acquired from multiple cortical areas and the hippocampus using NeuroGrid and a silicon probe, respectively. Shaded boxes highlight SPW-R (red), delta waves (gray), SPI (yellow), and CXR (blue). (Scale bar, 0.5 s.) (*C*) Sample recording traces from the hippocampus and PPC electrodes illustrating various hippocampal–cortical oscillatory interactions: SPW-R–CXR (*Top*; Scale bar, 60 ms), SPW-R–SPI (*Middle*; Scale bar, 0.5 s), and tripartite coupling (*Bottom*; Scale bar, 0.2 s.) (*D*) Sample CCGs between SPW-R–CXR (*Top*) and SPW-R–SPI (*Bottom*) during baseline NREM sleep (time 0 = occurrence of SPW-R; red lines indicate midpoint of upper and lower boundaries of 95% CIs shown as black-dotted lines; single session in one rat). Exclusive SPW-R–CXR CCG (*Top, Right*: 1,852 SPW-R and 1,892 CXR) was calculated by eliminating any CXR co-occurring with SPI in the inclusive CCG (*Top, Left*: 1,852 SPW-R and 2,805 CXR). Similarly, exclusive SPW-R–SPI CCG (*Bottom, Right*: 1,852 SPW-R and 968 SPI) was calculated by eliminating SPI co-occurring with CXR in the inclusive CCG (*Bottom, Left*: 1,852 SPW-R and 1,660 SPI). (*E*) Sample CCG between SPW-R, SPI, and CXR demonstrating tripartite coupling (time 0 = occurrence of SPW-R; single session in one rat; 1,852 SPW-R, 2,805 CXR, and 1,660 SPI). Parameter *a* represents the peak of the CCG at time 0, whereas *b* represents the average expected value at time 0. Coupling modulation (*M*) is calculated as (a-b)/b. (*F*) Group statistics demonstrating changes in coupling modulation (n = 6 rats, paired sample *t* test; *$P < 0.05$ between two groups). Significant difference between inclusive–exclusive SPW-R–SPI coupling modulation (orange; $P = 1.04 \times 10^{-4}$) but not inclusive–exclusive SPW-R–CXR coupling modulation (purple; $P = 0.324$). Gray lines show mean values for individual rats.

We determined the extent to which all three patterns were jointly correlated by identifying the CXR that co-occurred with SPI and performing cross-correlation with SPW-R (Fig. 1E). This tripartite coupling was statistically significant, and its strength was comparable to that of SPW-R–SPI coupling. Furthermore, when we eliminated SPI that were additionally coupled to CXR, the correlation between SPW-R–SPI significantly decreased (Fig. 1F). In contrast, significant SPW-R–CXR coupling was sustained despite elimination of SPI co-occurring with CXR (Fig. 1F). The relationship between CXR and SPI was also preserved under this manipulation (*SI Appendix*, Fig. S2). Taken together, these results suggest that hippocampal–cortical interactions in the absence of a consequential behavioral experience are dominated by SPW-R–CXR coupling but display joint modulation of SPW-R, CXR, and SPI.

We next asked how these oscillatory relationships were affected by behavioral experience sufficient to induce long-term memory. Both SPW-R–SPI and SPW-R–CXR coupling are altered by learning (24, 25), but whether these changes are manifestations of a unified underlying process and how their temporal dynamics modulate across memory phases remain unknown. To address these questions, we designed a behavioral protocol based on variations of the cheeseboard maze task [cheeseboard (CB) (33, 34); Movie S1]. This task is amenable to within-animal repetition,

with a robust new memory generated by changing the spatial locations associated with rewards. We leveraged this structure to examine dynamic memory processes within a consistent task schema. New memories for spatial locations were established with training trials, consolidated overnight, and then retrieved the following day in a set of test trials. Different reward locations were trained later the same day, initiating a subsequent memory cycle (Fig. 2A). We found that rats effectively sustained these memory cycles, with consistently high behavioral performance during retrieval the following day for each new memory. To evaluate the interaction between previously consolidated reward locations and new reward locations, we tracked the rat's trajectory across the maze during training (Fig. 2B). Initial training trials with new reward locations were characterized predominantly by searching at the previously rewarded locations. After an average of five trials, the rat shifted to a random searching strategy for new rewards, followed by subsequent trials consistent with gradual encoding of the new reward locations. Over the course of 15 to 20 trials, rats developed a stereotyped, efficient trajectory to navigate to the reward locations. Memory for these reward locations was successfully retrieved the subsequent day (Fig. 2C). These results demonstrate the rats' ability to flexibly, accurately, and repetitively generate new long-term memories based on the changing salient stimuli.
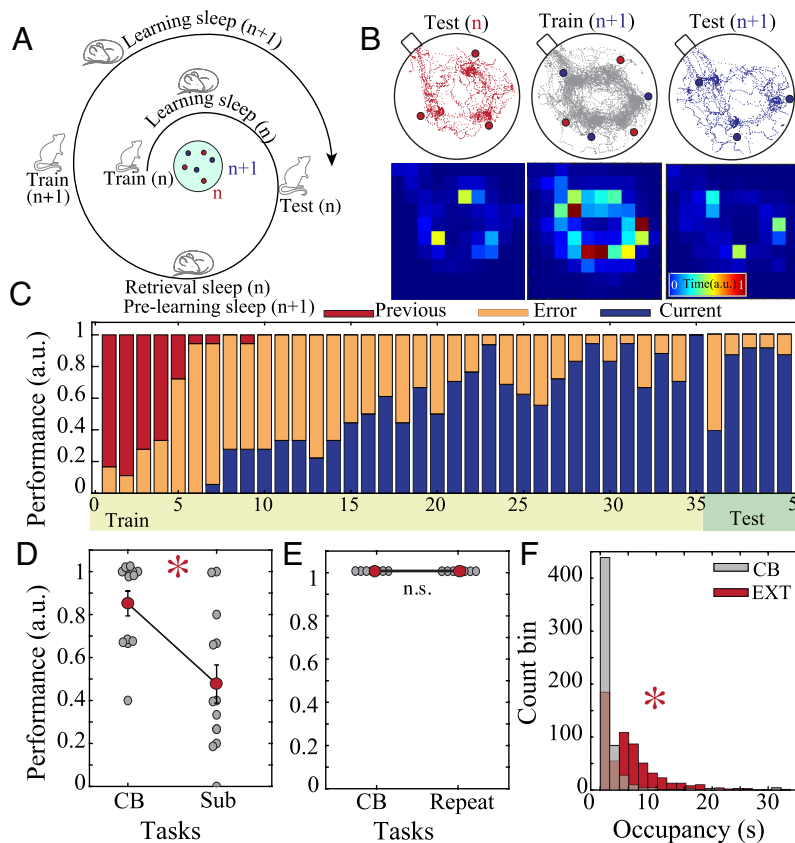

Fig. 2. Rats demonstrate the ability to flexibly update long-term memories in a spatial memory task. (A) Schematic of a behavioral protocol for the CB task. (B) Sample CB behavioral performance. *Top*: trajectory of a rat across the maze during five trials of test session$_{(n)}$ (red), during 25 trials of training session$_{(n+1)}$ (gray), and during five trials of test session$_{(n+1)}$ (blue). Red and blue circles indicate reward configuration$_{(n)}$ and reward configuration$_{(n+1)}$, respectively. *Bottom*: color map shows spatial distribution of time spent by the rat on the maze surface. Warmer colors represent the locations where the rat spent proportionally more time during the session. (C) Performance of rats across training and testing trials for the CB task (n = 6 rats). Red boxes represent the proportion of trials when the rats directly searched for the previously rewarded wells (reward configuration$_{(n)}$). Orange boxes represent the proportion of trials when the rats had a predominantly random exploration strategy. Blue boxes represent the proportion of trials where the rat directly navigated to the locations of currently rewarded wells (reward configuration$_{(n+1)}$). (D) Memory performance of rats was significantly decreased for subthreshold (sub) compared to regular CB training (paired t test, P = 0.003, n = 13 sessions). (E) Memory performance of rats was identical when the same reward configuration was used for two consecutive memory cycles (paired t test, P = 1, n = 7 sessions). (F) During extinction training sessions, rats spent more time exploring the maze compared to CB training sessions where rats spent minimum time in nonrewarded locations (K–S test, P << 0.001, n = 6 sessions).

We also designed several variations of the CB task to parse its component memory processes. First, we explored the relationship between extent of training and memory performance. Rats were trained on new reward locations only until they could demonstrate an accurate, effective navigation trajectory. After this truncated training session, rats were tested for recall of the reward locations the following day. We found that these sessions resulted in significantly impaired memory performance compared to completion of the full training session (Fig. 2D), indicating that a threshold of training must be attained to ensure robust formation of long-term memory. We next investigated the contrasting behavioral scenario by training rats on the same reward locations for two consecutive memory cycles. In this case of repeat learning, performance reached a plateau during the first memory cycle that was sustained throughout the subsequent training and testing sessions of the second memory cycle. Memory performance was not different between the first and second testing session, consistent with the notions that a single training session is sufficient to establish a robustly recalled long-term memory and that additional training does not further enhance behavior (Fig. 2E). Last, we conducted training sessions with the goal of extinguishing the previously recalled memory without encoding new reward locations. To accomplish this, we randomized reward locations on each training trial. Rats initially searched the previously recalled reward locations, but in the absence of rewards at these locations,

they then embarked on a random foraging strategy that resulted in a lack of stereotyped trajectory across the maze by the end of this session (SI Appendix, Fig. S3). In this manner, we were able to diminish the salience of the previous reward locations without introducing a novel learning demand (Fig. 2F).

These tasks allowed us to investigate how hippocampal–cortical communication is modulated across memory phases. Neurophysiological recordings were performed after each behavior session, and we analyzed the trajectory of oscillatory coupling during NREM sleep. To track changes within individual animals with sensitivity to each training–testing cycle, our analysis was based on comparisons between a sleep session and its chronologically subsequent sleep session, generating unique paired data points. Sleep quality was similar between sleep sessions that occurred after the different behavioral sessions (SI Appendix, Fig. S4), and we did not identify circadian patterns that could drive behavior-independent changes in oscillatory coupling (SI Appendix, Fig. S5). We first examined changes in SPW-R–CXR coupling as rats progressed through the memory cycle. We observed that this coupling was the strongest after a long-term memory was retrieved compared to when the memory was first established (Fig. 3 A and B). In contrast, SPW-R–CXR coupling was decreased by the transition from a previously learned reward configuration to a new reward configuration (Fig. 3 C and D). When we quantified this interaction at an intermediate time point during training, we found that
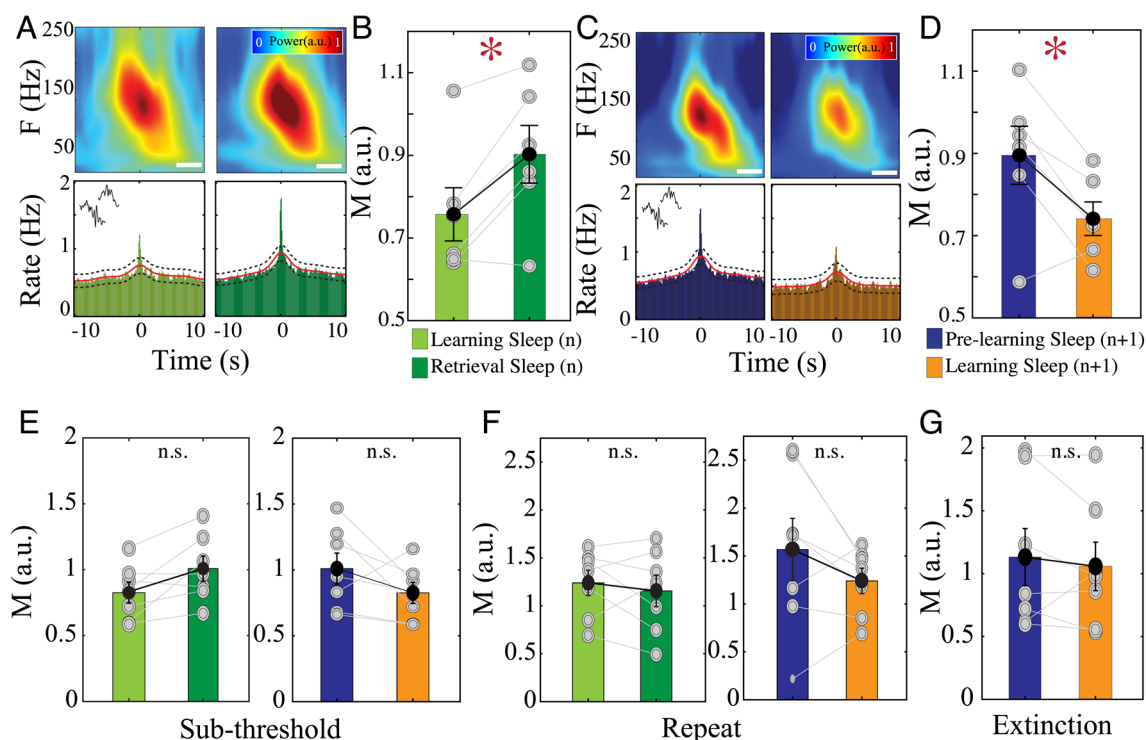

Fig. 3. Coupling of SPW-R with CXR is specifically up-regulated after retrieval of newly established long-term spatial memory. (A) PPC spectrogram trigger-averaged on occurrence time of SPW-R from sample rat (Top) reveals temporally locked increase in power in the ripple band that is more prominent in retrieval sleep$_{(n)}$ (Right) compared to that in learning sleep$_{(n)}$ (Left) on the CB task. Corresponding CCGs demonstrating change in SPW-R–CXR coupling (Bottom) during learning sleep$_{(n)}$ (Left: 1,555 SPW-R and 2,569 CXR) compared to that in retrieval sleep$_{(n)}$ (Right: 1,999 SPW-R and 4,263 CXR). Time 0 is the occurrence of SPW-R. (Scale bar, 25 ms.) (B) SPW-R–CXR coupling modulation in learning sleep$_{(n)}$ vs. retrieval sleep$_{(n)}$ (bars; mean ± SEM) on the CB task. Gray lines indicate the mean change in individual rats (n = 6 rats, paired t test, P = 0.0174* = P < 0.05). (C) PPC spectrogram trigger-averaged on occurrence time of SPW-R from sample rat (Top) reveals temporally locked increase in power in the ripple band that is more prominent in prelearning sleep$_{(n+1)}$ (Left) compared to that in learning sleep$_{(n+1)}$ (Right). Corresponding CCGs demonstrating change in SPW-R–CXR coupling (Bottom) during paired prelearning sleep$_{(n+1)}$ (Left: 1,936 SPW-R and 4,737 CXR) and learning sleep$_{(n+1)}$ stages (Right: 1,139 SPW-R and 1,662 CXR). (Scale bar, 25 ms.) (D) SPW-R–CXR coupling modulation in prelearning sleep$_{(n+1)}$ vs. learning sleep$_{(n+1)}$ on the CB task (n = 6 rats; paired t test, P = 0.028* = P < 0.05). (E) SPW-R–CXR coupling modulation on the subthreshold CB task variation for learning sleep$_{(n)}$ vs. retrieval sleep$_{(n)}$ (Left: n = 7 sessions, paired t test, P = 0.052) and prelearning sleep$_{(n+1)}$ vs. learning sleep$_{(n+1)}$ (Right: n = 7 sessions, paired t test, P = 0.16). (F) SPW-R–CXR coupling modulation on the repeat CB task variation for learning sleep$_{(n)}$ vs. retrieval sleep$_{(n)}$ (Left: n = 7 sessions, paired t test, P = 0.52) and prelearning sleep$_{(n+1)}$ vs. learning sleep$_{(n+1)}$ (Right: n = 7 sessions, paired t test, P = 0.23). (G) SPW-R–CXR coupling modulation on the extinction CB task variation for prelearning sleep$_{(n+1)}$ sleep vs. learning sleep$_{(n+1)}$ (n = 7 sessions, paired t test, P = 0.50).

SPW-R–CXR coupling progressively increased after additional learning trials and peaked after successful memory retrieval (*SI Appendix*, Fig. S6). The rats that underwent the subthreshold training (as in Fig. 2*D*) did not display significant changes in the SPW-R–CXR interaction, although trends were present that tracked the direction of change that occurred with a full training session (Fig. 3*E*). This pattern of modulation was specific for newly established long-term memory because repeat training of the previously learned and recalled reward locations (as in Fig. 2*E*) did not induce significant coupling modulation (Fig. 3*F*). An extinction training session (as in Fig. 2*F* and *SI Appendix*, Fig. S3) was also insufficient to change SPW-R–CXR coupling (Fig. 3*G*). In addition, the enhanced SPW-R–CXR coupling observed after memory retrieval occurred in the absence of a parallel increase in oscillation occurrence rates, indicating a specific alteration in temporal precision (*SI Appendix*, Fig. S7). Taken together, these results demonstrate that long-term memory processes drive phase-specific modulations in SPW-R–CXR coupling.

We next examined SPW-R–SPI coupling across the memory cycle. In contrast to SPW-R–CXR coupling, we found that this coupling was significantly increased after learning but dropped after retrieval (Fig. 4 *A–D*). These changes were enhanced when instances of tripartite coupling were eliminated in contrast to what was observed in the absence of memory demand (Fig. 4 *B* and *D*). Behavioral experiences that i) were subthreshold for long-term memory expression, ii) repeated previously trained information, or iii) served to extinguish previous memory in the absence of new information were all insufficient to generate significant changes in SPW-R–SPI coupling (Fig. 4 *E–G*).

Although occurrence rates of SPW-R and SPI paralleled their coupling modulation across the memory cycle, the precise oscillatory pairing exceeded that predicted by rate (*SI Appendix*, Fig. S7). Thus, SPW-R–SPI coupling is strongly induced by long-term memory with a different time course across memory phases compared to SPW-R–CXR coupling. Of note, the direct interaction between CXR and SPI did not change with any memory phase (*SI Appendix*, Fig. S8).

To investigate how these oscillatory coupling patterns could be influenced by the type of task, we conducted similar analyses for a nonspatial object association task [object association (OA) (35)]. Rats learned to associate a particular object with a reward over the course of training trials and successfully retrieved memory for this object the following day (Fig. 5 *A* and *B* and Movie S1). Similar to our findings with the CB task, SPW-R–CXR coupling was significantly increased during sleep following retrieval compared to learning (Fig. 5*C*). This change was also specific for new information because it was abolished by repeating the same object–reward association on consecutive memory cycles (Fig. 5*D* and *SI Appendix*, Fig. S9). However, significant alteration of SPW-R–SPI coupling was not observed for any stage of this memory task (Fig. 5 *E* and *F*). These results suggest a conserved role for SPW-R–CXR in long-term memory but a task-specific function of SPW-R–SPI coupling.

Given these findings, we further characterized the dynamics of SPW-R–CXR coupling across individual sleep sessions after behavior on the CB and OA tasks. We found that in the sleep session after learning for both the spatial and nonspatial tasks, coupling rates were initially high but exhibited a steady decline
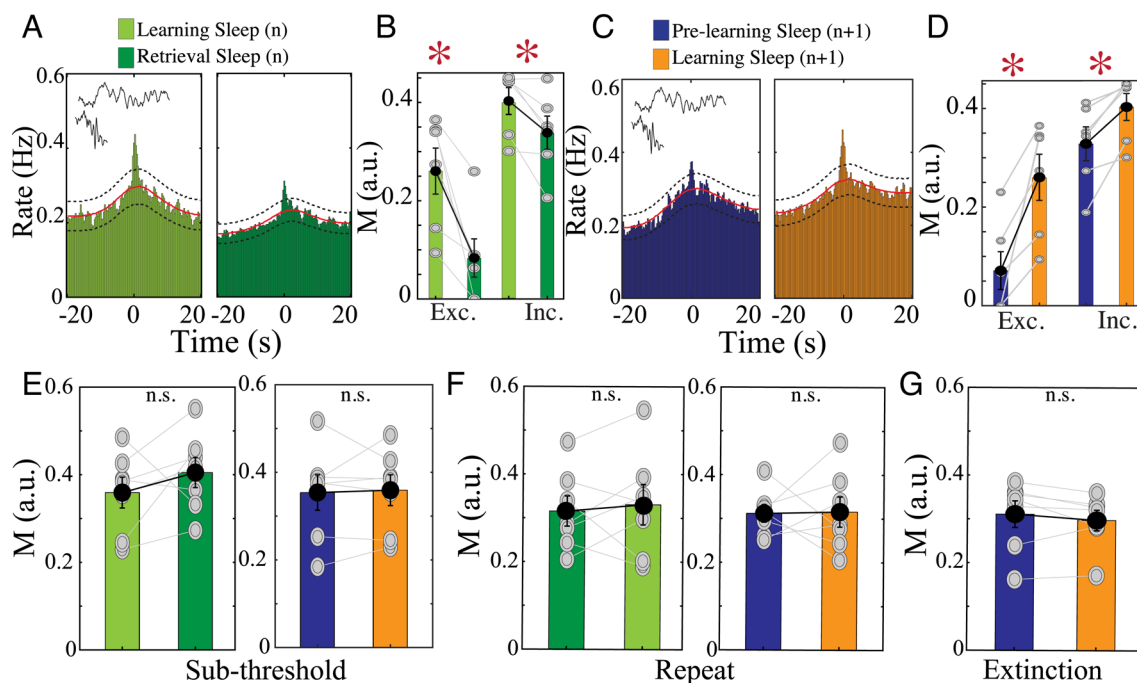

Fig. 4. Coupling of SPW-R with SPI is specifically up-regulated after learning of newly established long-term memory. (*A*) Sample SPW-R–SPI CCGs demonstrating a decrease in modulation during retrieval sleep$_{(n)}$ (*Left*: 1,668 SPW-R and 1,312 SPI) vs. learning sleep$_{(n)}$ (*Right*: 2,025 SPW-R and 1,353 SPI) on the CB task. (*B*) Significant change in coupling modulation between learning sleep$_{(n)}$ and retrieval sleep$_{(n)}$ for exclusive and inclusive SPW-R–SPI coupling on the CB task (*Left*: exclusive, $P = 0.0127$; *Right*: inclusive, $P = 0.032$; paired t test, *$P < 0.05$; n = 6 rats). (*C*) Sample SPW-R–SPI CCGs demonstrating an increase in modulation during learning sleep$_{(n+1)}$ (*Left*: 1,473 SPW-R and 1,009 SPI) vs. prelearning sleep$_{(n+1)}$ (*Right*: 1,318 SPW-R and 1,020 SPI) on the CB task. (*D*) Significant change in coupling modulation between prelearning sleep$_{(n+1)}$ and learning sleep$_{(n+1)}$ for exclusive (*Left*: paired t test, $P = 0.012$) and inclusive (*Right*: paired t test, $P = 0.010$) SPW-R–SPI coupling on the CB task. *$P < 0.05$; n = 6 rats. (*E*) SPW-R–SPI coupling modulation on the subthreshold CB task variation for learning sleep$_{(n)}$ vs. retrieval sleep$_{(n)}$ (*Left*: n = 7 sessions, paired t test, $P = 0.33$) and prelearning sleep$_{(n+1)}$ vs. learning sleep$_{(n+1)}$ (*Right*: n = 7 sessions, paired t test, $P = 0.82$). (*F*) SPW-R–SPI coupling modulation on the repeat CB task variation for learning sleep$_{(n)}$ vs. retrieval sleep$_{(n)}$ (*Left*: n = 7 sessions, paired t test, $P = 0.69$) and prelearning sleep$_{(n+1)}$ vs. learning sleep$_{(n+1)}$ (*Right*: n = 7 sessions, paired t test, $P = 0.92$). (*G*) SPW-R–SPI coupling modulation on the extinction CB task variation for prelearning sleep$_{(n+1)}$ sleep vs. learning sleep$_{(n+1)}$ (n = 7 sessions, paired t test, $P = 0.32$).
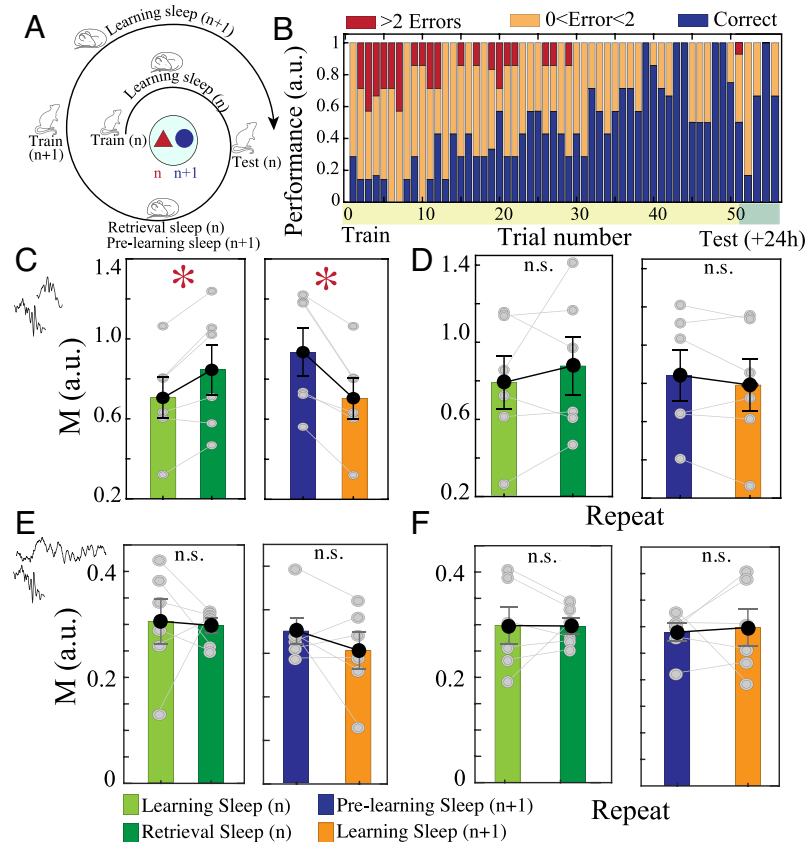
Fig. 5. Coupling of SPW-R with CXR is specifically up-regulated after retrieval of established long-term nonspatial memory. (*A*) Schematic of a behavioral protocol for a nonspatial object association (OA) task. (*B*) Performance of rats across training and testing trials for the OA task (n = 6 rats). Red boxes indicate proportions of trials where rats explored >2 incorrect reward objects before finding the correct object. Orange boxes indicate trials where rats explored at most two incorrect objects. Blue boxes represent the proportion of trials where rat directly located the correct object. (*C*) SPW-R–CXR coupling modulation in learning sleep$_{(n)}$ vs. retrieval sleep$_{(n)}$ (*Left*: paired *t* test, *P* = 0.019) and prelearning sleep$_{(n+1)}$ vs. learning sleep$_{(n+1)}$ (*Right*: paired *t* test, *P* = 0.0067) on the OA task. Gray lines indicate the mean change in individual rats (bars; mean ± SEM; n = 6 rats, *= *P* < 0.05). (*D*) SPW-R–CXR coupling modulation in the repeat variation of the OA task for learning sleep$_{(n)}$ vs. retrieval sleep$_{(n)}$ (*Left*: paired *t* test, *P* = 0.47) and prelearning sleep$_{(n+1)}$ vs. learning sleep$_{(n+1)}$ (*Right*: paired *t* test, *P* = 0.28). (*E*) SPW-R–SPI coupling modulation in learning sleep$_{(n)}$ vs. retrieval sleep$_{(n)}$ (*Left*: paired *t* test, *P* = 0.87) and prelearning sleep$_{(n+1)}$ vs. learning sleep$_{(n+1)}$ (*Right*: paired *t* test, *P* = 0.30) on the OA task. (*F*) SPW-R–SPI coupling modulation in the repeat variation of the OA task for learning sleep$_{(n)}$ vs. retrieval sleep$_{(n)}$ (*Left*: paired *t* test, *P* = 0.47) and prelearning sleep$_{(n+1)}$ vs. learning sleep$_{(n+1)}$ (*Right*: paired *t* test, *P* = 0.29).

over subsequent NREM sleep (Fig. 6 *A* and *B*, light colors). In contrast, the sleep after retrieval of a spatial or nonspatial long-term memory was associated with a similar initial peak but then a sustained plateau in coupling (Fig. 6 *A* and *B*, dark colors). These data indicate that the temporal recruitment of SPW-R–CXR coupling is time limited and specific to whether memory was previously encoded or retrieved. We then aimed to synthesize these results into neural signatures characteristic of different stages within the memory cycle. We classified changes that occurred after learning and prior to retrieval as related to consolidation and changes that occurred after retrieval but prior to any new learning as reconsolidation. For CB and OA tasks, the principal indicator of reconsolidation was a surge in SPW-R–CXR coupling. This increase was accompanied by a decrease in SPW-R–SPI coupling that was only significant for the CB task. In contrast, consolidation was characterized by enhancement of SPW-R–SPI coupling for the CB task only. Unsupervised k-means clustering based on SPW-R–CXR and SPW-R–SPI coupling modulations resulted in an accurate classification of memory processes across animals (Fig. 6*C*). When examined chronologically, these patterns resulted in a cyclic, task-specific modulation of oscillatory coupling that was appreciable at the level of an individual rat (Fig. 6 *C* and *D*). Therefore, hippocampal–cortical communication occurs in independent streams that are differentially modulated by both the memory phase and the spatial demand of the task. These results

support the notion that oscillatory coupling facilitates memory-specific information flow and shed light onto the mechanisms that govern long-term memory in a dynamic environment.

Discussion

Here, we investigated oscillatory dynamics between the hippocampus and cortex as long-term memories were consolidated, strengthened, and updated during sleep after a behavioral experience. We found that in the absence of memory demand, SPW-R, CXR, and SPI were jointly modulated in these regions. Offline consolidation of spatial, but not nonspatial, memory was correlated with independent recruitment of SPW-R–SPI coupling. Subsequent retrieval and reconsolidation initiated a shift toward enhanced SPW-R–CXR interactions for both memory types. This shift only occurred for recently established long-term memories; in the absence of new learning within 24 h, no changes were evoked. The stage of memory processing could be identified by the relative prominence of oscillatory coupling patterns and their postbehavior dynamics. These findings suggest the ability of such interactions to specifically, flexibly, and repetitively support memory processes required for adaptation to a changing environment.

Memory consolidation requires protein synthesis (36, 37), and reactivation of a previously consolidated memory is postulated to restore its lability, as demonstrated by an additional window of
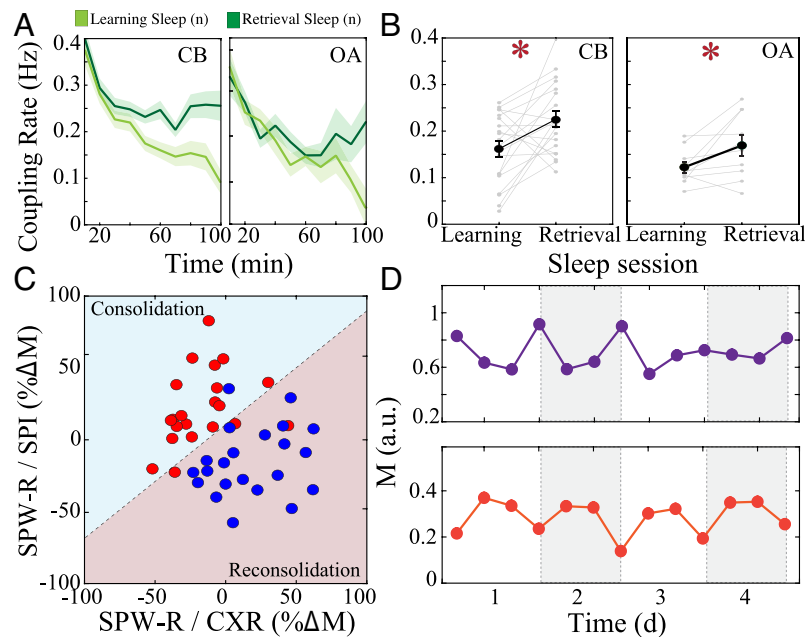
Fig. 6. Memory consolidation and reconsolidation are differentiable on the basis of hippocampal–cortical coupling patterns. (*A*) Joint occurrence rate of SPW-R and CXR across NREM sessions reveals different temporal trajectories for learning sleep$_{(n)}$ vs. retrieval sleep$_{(n)}$ on the CB task (*Left*: n = 23 sessions) and the OA task (*Right*: n = 12 sessions). Lines and shaded bars represent mean ± SEM (*B*) Increase in joint occurrence rate of SPW-R and CXR from learning sleep$_{(n)}$ vs. retrieval sleep$_{(n)}$ on the CB task (*Left*: n = 20 sessions; paired t test, P = 0.012) and OA task (*Right*: n = 10 sessions; paired t test, P = 0.037). Data represented as mean ± SEM; gray lines are individual sessions; *P < 0.05. (*C*) Unsupervised k-means clustering of the percentage changes in the coupling modulation of SPW-R–CXR and SPW-R–SPI between sleep sessions after memory phases on the CB task shows accurate classification (n = 6 rats, accuracy = 86.36%). (*D*) Cyclical modulation of SPW-R–CXR coupling (*Top*) and SPW-R–SPI coupling (*Bottom*) across the memory cycle for the CB task (sample rat).

susceptibility to protein synthesis blockade in certain conditions (38–40). These processes are partially differentiable on the basis of identified molecular mechanisms and involved anatomical circuits (4, 41, 42). Our data, which demonstrate a contrast between hippocampal–cortical oscillatory interactions after learning and retrieval, support the notion that these experiences can be functionally and mechanistically distinguished. Furthermore, we observed that a retrieval experience characterized by reinforcement of previous associations resulted in a different pattern of oscillatory coupling than a retrieval experience that weakened previous associations and established new ones within the same schema. Such patterns may therefore provide insight into whether a behavioral experience has served to strengthen or extinguish a memory. Repetitive training and retrieval of the same associations over 2 d eliminated oscillatory coupling differences during the subsequent offline epochs, suggesting either a time-limited role in both consolidation and reconsolidation or a requirement for proximal new learning. Further behavioral experiments that extend the examination of an individual memory could facilitate disambiguation of these possibilities.

Significant modification of hippocampal–cortical coupling occurred with spatial and nonspatial tasks, in keeping with evidence supporting the role for the hippocampus and distributed cortical regions in offline processing for both these types of memory (14, 43, 44). However, SPW-R–SPI coupling was more strongly modulated across consolidation and reconsolidation of the spatial, compared to the nonspatial, task. We propose that this form of coupling is most prominent with the PPC for tasks that heavily rely on spatial context information (30, 45), whereas SPW-R–CXR coupling is more generally activated within complex, distributed circuits involved in strengthening of long-term representations (46, 47). It is possible that this SPW-R–SPI coupling is locally up-regulated in cortical regions outside of the PPC during the nonspatial task.

In keeping with previous studies, we found that occurrence rates of SPW-R and SPI were modestly modulated by previous salient behavioral experiences (48–52). However, we found evidence to support independent regulation of oscillation occurrence rate and temporal coupling. Changes in coupling strength utilized were selected to normalize for rate measures (53, 54), and during specific memory stages, coupling strength was increased when oscillation occurrence rate decreased. Because SPW-R, CXR, and SPI have all individually been associated with reactivation of behaviorally relevant neural spiking patterns and cellular plasticity (17, 55–57), these parameters could be differentially engaged to modify local or distributed processes depending on the memory phase and task demand.

Rodents established long-term memory for our tasks in a single day of training and efficiently updated these memories within a previously learned schema when reward associations were changed. This task structure allowed us to focus on the dynamics of the memory process in contrast to tasks where prolonged training requirements, strong aversive responses, or habituation can hinder repeated cycles of memory formation within an individual animal (33, 34, 58). Oscillation occurrence rates and strength of oscillatory coupling demonstrated memory-driven fluctuation around a set point, suggestive of homeostatic limits on modulation of these parameters over the course of days. On a shorter timescale, coupling was the highest in the sleep epochs immediately following a behavior, consistent with the effectiveness of closed-loop manipulations performed for only the first hour of the consolidation period in modifying memory and evidence for rapid establishment of cortical engrams (22, 24, 30, 59). During reconsolidation, SPW-R–CXR coupling was also increased in later sleep epochs, raising a potential parallel with the delayed window of memory-modulating effects for cortically administered pharmacologic substances (60–62).

The fate of a long-term memory is determined by subsequent experience and is dynamic over a prolonged period. Our results show that three prominent network patterns implicated in memory (SPW-R, SPI, and CXR) undergo dynamic comodulation across the cycle of memory consolidation, reconsolidation, and updating. We hypothesize that temporal links between these plasticity-related oscillations in different brain structures provide the network infrastructure for cellular and molecular changes associated with long-term memory processing. These oscillatory coupling patterns present an opportunity for design of novel closed-loop investigations to manipulate memory across distributed neural networks and enhance understanding of disorders characterized by impaired and overactive information retention (63, 64).

Materials and Methods

Probe Fabrication and Preparation. The fabrication of conducting polymer-based Neuro Grids has been discussed in previous publications (25, 65). In brief, a projection exposure system was used to pattern parylene C, Au, Pt, Ti, and poly (3,4-ethylenedioxythiophene) polystyrene sulfonate (PEDOT:PSS) films. The NeuroGrid was attached to a custom-printed circuit board using mixed-conducting particulate composites (66). The board contained an RHD2164 die (Intan Technologies) for the purpose of amplification, digitization, and transmission of the acquired neural signals via a serial peripheral interface protocol to a computer interface board (RHD2000 evaluation board; Intan Technologies). All back-end electronics were covered with silicone elastomer as an encapsulation layer.

Animal Surgical Procedure. All animal experiments were approved by the Institutional Animal Care and Use Committee at the Columbia University. Nine male Long Evans rats (200 to 350 g) were used for intracranial implantation. Rats were kept on a regular 12-h–12-h light–dark cycle and housed in pairs prior to implantation but separated afterward. Prior experimentation was not performed on these animals. The animals were initially anesthetized with 2% isoflurane and maintained under anesthesia with 0.75 to 1% isoflurane during surgery. Silicon probes and/or wires were implanted into the hippocampus (−3.5 anterior-posterior (AP) and 3.0 medial-lateral (ML)). A NeuroGrid electrocorticography array was placed over the dorsal cortical surface of the contralateral hemisphere relative to the wires. Screws in the skull, overlying the cerebellum, served as ground electrodes. The craniotomies were covered by Gelfoam and sealed using a 10:1 mixture of paraffin and mineral oil. Rats recovered for 4 to 5 d prior to initiation of experimentation. Hippocampal electrodes were adjusted in the dorsal–ventral axis to target the CA1 pyramidal cell layer based on characteristic appearance of hippocampal SPW-Rs.

Neurophysiology Data Acquisition and Processing. All rats underwent a protocol consisting of neurophysiological recordings and behavioral tasks. Recordings were started at a fixed time, timed after each behavioral intervention. Neurophysiological signals were amplified, digitized continuously at 20 kHz using a headstage directly attached to the probe (RHD2000; Intan Technologies), and stored for offline analysis with 16-bit format. Data were analyzed using MATLAB (MathWorks) and visualized using Neuroscope.

Behavioral Training. Rats were placed on a water deprivation schedule for 3 to 5 d prior to intracranial implantation to ensure they could receive water through a handheld syringe. Rats were weighed daily during water deprivation to ensure that body weight did not decrease to <85% of predeprivation measurements. Three additional rats underwent only behavioral training.

Behavior for all tasks was tested on a cheeseboard maze consisting of a 1.5-m-diameter open circular arena that was painted a uniform green and stood 70 cm above the floor. A total of 177 water wells (7 mm in diameter and 3 mm in depth) were drilled 8 cm apart in the maze surface, forming evenly distributed, parallel columns and rows. One wall of the starting box (23 cm wide × 30 cm long × 48 cm high) functioned as a gate that could be raised and lowered to control the rat's access to the maze.

Prior to surgery, water-deprived rats were first familiarized with exploring the maze environment to obtain water. Initially, the rat was placed in the center of the maze and allowed to explore and retrieve multiple (~25) randomly placed hidden water rewards. Over the next 3 d, the number of available water rewards on the maze was gradually reduced, and a trial structure was

introduced such that the rat received a food reward (0.5 to 1 Froot Loop) after successful retrieval of all water rewards. The rat was then trained to return to the starting box after retrieving water to obtain its food reward. After 2 to 4 d of this repeated procedure, the rat would consistently explore the maze to obtain three spatially distinct water rewards and then independently return to the starting box. To prevent use of odor-mediated searching, the maze was wiped with a towel soaked in 70% ethanol and rotated by a random multiple of 90° relative to the starting box between all trials. Plastic toys of varying shapes and colors were then introduced onto the maze surface. Rats were exposed to the objects initially to ensure that there were no intrinsic preferences for any given object. Rats learned to displace the objects and obtain water from the well directly under the object. This phase of general training ended when the rat could complete 35 to 50 trials per day. Behavior sessions were monitored by an overhead video camera (20 fps), and tracking of the rat's location was facilitated by blue and red light emitting diodes (LEDs) attached to its cap. Rats had neurophysiological recording in their home cage after each behavioral session. Several rats performed both CB and OA tasks, with each rat typically completing 2 to 4 memory cycles per task.

Cheeseboard Maze Task. Each memory cycle on this task was completed over 2 d. On the first of the 2 d, the rats learned the location of three hidden water rewards placed in a randomly selected set of 3 water wells over the course of ~35 trials (25 trial sessions, then ~1-h home cage rest, and then 10 trial sessions). All rats obtained >80% performance averaged over five trials by the end of the training session. On the second of the 2 d, the rat was given a five-trial test with water rewards located in the same location as the first day to assess memory for the spatial configuration of the reward locations. After 4 h in the home cage, the rat was brought back to the maze to learn three different water reward locations. Behavior was scored by tracking the animal's trajectory across the maze. During training sessions, the trajectory was compared to that of the test session performed earlier in the day (wherein the rat tracks to the previous day's rewards) and an idealized minimal distance trajectory between the new reward locations. Memory performance in the test session was scored by determining the number of rewards obtained in <30 s per trial, weighted by trial number (with higher weight to the initial trials).

Object Association Task. On the first day for this task, rats learned to associate one of five objects placed at random locations on the cheeseboard maze surface over the course of ~50 trials. The number of trials and temporal arrangement were slightly modified compared to those of the CB task due to different amounts of water obtained by the rat per trial (affecting motivational status) and number of trials required to meet the learning criterion (> 80% performance averaged over five trials). On the second day, the rat was given a 5-trial test with water rewards associated with the same object as the first day to assess this memory. After 4 h in the home cage, the rat was brought back to the maze to complete another training session, which consisted of either a new object–reward association or retraining with the same object–reward association from the previous day. Behavior was scored by tracking the animal's interactions with the objects. Direct navigation to the correct object was scored the highest, with progressively lower scores for each incorrect object explored prior to the correct object.

Task Variations. A series of variations on the behavioral protocols were conducted.

Subthreshold. A subthreshold memory cycle took place over 3 d. The first day consisted of a normal CB task training followed by a test session on the morning of the second day. Approximately 4 h after this test session, a single "subthreshold" training session was performed. In subthreshold training, the animal was taught a new spatial reward configuration but with fewer training trials. Once the animal was able to successfully navigate to all reward locations on three consecutive trials in <30 s, the session was terminated, and the animal was placed in the home cage to sleep. On the third day, the animal was tested on the reward configuration used in the subthreshold training.

Repeat. In this case, the animal was trained on reward configurations that had been used in the previous training/testing sessions. Performance was assayed by a subsequent test session the following day.

Extinction. An extinction cycle took place over 2 d. The first day consisted of a normal CB task training followed by a test session on the morning of the second day. Approximately 4 h after this test session, a single "extinction" training session was performed. In extinction training, the general task structure was unchanged, but reward locations were randomized for each individual trial of the session. The trials were continued until the animal consistently no longer navigated in a directed manner to the reward locations from the previous training/testing sessions and instead foraged the maze randomly. Use of the reward locations from previous training/testing sessions was avoided during reward location randomization to prevent reinforcement of the prior trajectory.

Preprocessing. The electrophysiological data were resampled to 1,250 Hz to facilitate local field potential (LFP) analysis. We identified epochs of sleep by first detecting immobility in the motion signal of the accelerometer attached to the headstage and absence of electromyogram (EMG) artifacts. NREM sleep epochs were then detected by locating periods of elevated delta (0.5 to 4 Hz) amplitude in the neocortex at times of immobility. rapid eye movement sleep (REM)M epochs were distinguished by an increased theta–delta-band frequency ratio in the intracranial electroencephalography (iEEG) spectrograms in the hippocampus. Sleep-scored epochs were then visually inspected and manually adjusted using whitened spectrograms and raw traces to eliminate short epochs containing movement artifacts.

Region Selection. The anatomical location of each NeuroGrid electrode was estimated by first determining the stereotactic position of the anteromedial electrode, which sits closest to bregma. Then by following the interchannel distance, we interpolated the anatomical position of each electrode based on the rat stereotactic atlas. We corroborated these anatomical regions with physiological markers. Electrodes demonstrating a high rate of CXRs overlapped with channels marked as the PPC based on anatomical mapping. Only the detected events in the channels identified in the PPC region were considered for analysis. We visually inspected the recordings in Neuroscope to eliminate noisy electrodes.

LFP Event Detection. SPW-R, SPI, and CXR were detected based on the Freely Moving Animal (http://fmatoolbox.sourceforge.net) toolbox sequential detection algorithm. Detection of SPW-R was initiated by visually determining a channel where SPW-R were present and then band-pass filtering this hippocampal channel between 100 and 250 Hz. The filtered signal was then rectified and instantaneous power was extracted using the Hilbert transform. Events where the filtered envelope was two SDs above the baseline SD of the filtered traces and where peaks reached five times the SD were selected. Only events longer than 20 ms duration were selected, and the duration between two SPW-R events had to be a minimum of 30 ms. Events common to the ripple channel and an EMG electrode noise channel were eliminated.

To detect SPI in the PPC, a PPC channel was filtered between 10 and 20 Hz, followed by signal rectification and enveloping. Events where the filtered envelope was greater than 3 SD above the baseline for a minimum of 300 ms and a maximum of 4 s were detected. The duration between two SPI events had to be a minimum of 450 ms.

CXR were detected by filtering a PPC channel between 110 and 180 Hz, rectifying and extracting instantaneous power using the Hilbert transform. CXR were identified when the envelope was greater than 5 SD above the baseline for a minimum of 20 ms and a maximum of 90 ms. The duration between two CXR events was set to a minimum of 30 ms. All detections were visually inspected for accuracy for each recording session.

Rate Calculation. The rate of SPW-R was calculated by dividing the number of detected SPW-R in the hippocampal channel by the duration of NREM sleep. For CXR and SPI, the detected events were pooled together from all the PPC channels, and any repeating event time points were eliminated. This allowed us to identify all the unique events occurring in the PPC region. Dividing the number of unique events by the NREM duration provided us with the rate of CXR and SPI.

Cross-correlograms (CCG) Calculation. To determine coupling between detected oscillations, CCGs were calculated, and the statistical significance was determined using a modified convolution method (53). The CCG was calculated from the counts of the underinvestigation event E_2 at specific time delays with respect to the occurrence of the reference event E_1 which quantifies the temporal correlation between two detected events.

By convolving the cross-correlation histogram with a partially hollowed window, we estimated the co-occurrence of the two events when the occurrence of the two events is independent (54). The CI was estimated from a Poisson distribution with the mean lambda value determined from the convolution.

The peak of the CCG (a) above the CI and expected value level (b) at time zero allow us to compute the coupling modulation (M) as a normalized ratio of the peak exceeding the CI at chance.

$$M = \frac{a - b}{b}.$$

Consider the scenario where the entire length of neural recording was divided into time bins without overlap. For each time bin, suppose that E_2 occurs with a probability p_1 if event E_1 is present but with probability p_2 if event E_1 is absent. The degree of difference of the two probabilities can be quantified through the log odds ratio (R) (54) as follows:

$$R = \log \left(\frac{p_1}{1 - p_1} \bigg/ \frac{p_2}{1 - p_2} \right),$$

where the statistical parameter R quantifies the tendency of the two events to co-occur. In our case, both p_1 and p_2 are much lower than 1 based on the small time bins comprising the CCG compared to the length of the entire recording. The ratio can then be simplified as follows:

$$R = \log \left(\frac{p_1}{p_2} \right).$$

From the CCG, probabilities p_1 and p_2 are directly proportional to the significant number of co-occurring events per second a and the number of co-occurring events at chance b, respectively.

$$\frac{p_1}{p_2} \propto \frac{a}{b}.$$

The coupling strength we defined can be seen as equivalent to the exponential of co-occurrence index R with a shift (a/b-1). The coupling strength thus quantifies the co-occurrence of two events and is independent of the occurrence rate of both event 1 and event 2.

To determine validity across different statistical approaches, we compared CCG quantification with another methodology demonstrated to reliably assess correlation (affinity metric) as described in ref. 54. Both CCG quantification and the affinity metric account for oscillation occurrence rates and gave concordant results. Joint occurrence rates of oscillations do not only account for oscillation occurrence rates but also demonstrate similar directional modulation in a subset of data tested (*SI Appendix*, Fig. S10). CCG quantification was selected as an appropriate statistical representation of oscillatory coupling and used for all analyses.

CCG Dynamics across Sleep Epochs. To examine the dynamics of SPW-R–CXR coupling over sleep, we looked at events occurring within every 10 min, non-overlapping NREM window across the entire recording session with the NREM duration longer than 80 min. We calculated the co-occurrence by counting the number of SPW-R and CXR events that coincided temporally within 100 ms of their peak times. We divided the count by the nominal occurrence rate of SPW-R.

Statistics. We conducted statistical analyses across the different memory sleep stages following training or test sessions for both CB and OA tasks. To test the null hypothesis that there is no significant difference in the coupling strength between memory stages, we used paired t test. Kolmogorov–Smirnov (K–S) testing was used to compare distributions. Significance was taken as $P < 0.05$. The unsupervised k-means algorithm was used to cluster patterns of oscillatory coupling modulation.

Data, Materials, and Software Availability. All study data are included in the article and/or *SI Appendix*.

1. J. L. McGaugh, Memory - A century of consolidation. *Science* **287**, 248–251 (2000).
2. K. Nader, G. E. Schafe, J. E. le Doux, The labile nature of consolidation theory. *Nature* **1**, 216–219 (2000).
3. C. M. Alberini, Mechanisms of memory stabilization: Are consolidation and reconsolidation similar or distinct processes? *Trends Neurosci* **28**, 51–56 (2005).
4. J. L. C. Lee, B. J. Everitt, K. L. Thomas, Independent cellular processes for hippocampal memory consolidation and reconsolidation. *Science* **304**, 839–843 (2004).
5. J. L. C. Lee, Reconsolidation: Maintaining memory relevance. *Trends Neurosci.* **32**, 413–420 (2009).
6. H. Eichenbaum, A cortical–hippocampal system for declarative memory. *Nat. Rev. Neurosci.* **1**, 41–50 (2000).
7. M. G. Zhao *et al.*, Roles of NMDA NR2B subtype receptor in prefrontal long-term potentiation and contextual fear memory. *Neuron* **47**, 859–872 (2005).
8. T. Kitamura, S. K. Ogawa, D. S. Roy, T. Okuyama, Engrams and circuits crucial for systems consolidation of a memory. *Science* **356**, 73–78 (2017).
9. T. Okuyama, T. Kitamura, D. S. Roy, S. Itohara, S. Tonegawa, Ventral CA1 neurons store social memory. *Science* **353**, 1536–1541 (2016).
10. J. J. Quinn, Q. D. Ma, M. R. Tinsley, C. Koch, M. S. Fanselow, Inverse temporal contributions of the dorsal hippocampus and medial prefrontal cortex to the expression of long-term fear memories. *Learn. Mem.* **15**, 368–372 (2008).
11. J. Lopez *et al.*, Context-dependent modulation of hippocampal and cortical recruitment during remote spatial memory retrieval. *Hippocampus* **22**, 827–841 (2012).
12. T. Maviel, T. P. Durkin, F. Menzaghi, B. Bontempi, Sites of neocortical reorganization critical for remote spatial memory. *Science* **305**, 96–99 (2004).
13. P. W. Frankland, B. Bontempi, L. E. Talton, L. Kaczmarek, A. J. Silva, The involvement of the anterior cingulate cortex in remote contextual fear memory. *Science* **304**, 881–883 (2004).
14. A. Sawangjit *et al.*, The hippocampus is crucial for forming non-hippocampal long-term memory during sleep. *Nature* **564**, 109–113 (2018).
15. L. R. Squire, Memory and the hippocampus: A synthesis from findings with rats, monkeys, and humans. *Psychol. Rev.* **99**, 195–231 (1992).
16. A. Peyrache, M. Khamassi, K. Benchenane, S. I. Wiener, F. P. Battaglia, Replay of rule-learning related neural patterns in the prefrontal cortex during sleep. *Nat. Neurosci.* **12**, 919–926 (2009).
17. D. Mao *et al.*, Hippocampus-dependent emergence of spatial sequence coding in retrosplenial cortex. *Proc. Natl. Acad. Sci. U.S.A.* **115**, 8015–8018 (2018).
18. M. P. Walker, R. Stickgold, Sleep-dependent learning and memory consolidation. *Neuron* **44**, 121–133 (2004).
19. B. P. Staresina *et al.*, Hierarchical nesting of slow oscillations, spindles and ripples in the human hippocampus during sleep. *Nat. Neurosci.* **18**, 1679–1686 (2015).
20. D. R. Euston, M. Tatsuno, B. L. McNaughton, Fast-forward playback of recent memory sequences in prefrontal cortex during sleep. *Science* **318**, 1147–1150 (2007).
21. M. A. Wilson, B. L. McNaughton, Reactivation of hippocampal ensemble memories during sleep. *Science* **265**, 676–679 (1994).
22. G. Girardeau, K. Benchenane, S. I. Wiener, G. Buzsáki, M. B. Zugaro, Selective suppression of hippocampal ripples impairs spatial memory. *Nat. Neurosci.* **12**, 1222–1223 (2009).
23. S. P. Jadhav, C. Kemere, P. W. German, L. M. Frank, Awake hippocampal sharp-wave ripples support spatial memory. *Science* **336**, 1454–1458 (2012).
24. N. Maingret, G. Girardeau, R. Todorova, M. Goutierre, M. Zugaro, Hippocampo-cortical coupling mediates memory consolidation during sleep. *Nat. Neurosci.* **19**, 959–964 (2016).
25. D. Khodagholy, J. N. Gelinas, G. Buzsáki, Learning-enhanced coupling between ripple oscillations in association cortices and hippocampus. *Science (1979)* **358**, 369–372 (2017).
26. A. P. Vaz, S. K. Inati, N. Brunel, K. A. Zaghloul, Coupled ripple oscillations between the medial temporal lobe and neocortex retrieve human memory. *Science* **363**, 975–978 (2019).
27. C. Sestieri, M. Corbetta, G. L. Romani, G. L. Shulman, Episodic memory retrieval, parietal cortex, and the default mode network: Functional and topographic analyses. *J. Neurosci.* **31**, 4407–4420 (2011).
28. C. S. Keene, D. J. Bucci, Contributions of the retrosplenial and posterior parietal cortices to cue-specific and contextual fear conditioning. *Behav. Neurosci.* **122**, 89–97 (2008).
29. J. L. Rogers, R. P. Kesner, Hippocampal-parietal cortex interactions: Evidence from a disconnection study in the rat. *Behav. Brain Res.* **179**, 19–27 (2007).
30. S. Brodt *et al.*, Fast track to the neocortex: A memory engram in the posterior parietal cortex. *Science* **362**, 1045–1048 (2018).
31. A. Sirota, J. Csicsvari, D. Buhl, G. Buzsáki, Communication between neocortex and hippocampus during sleep in rodents. *Proc. Natl. Acad. Sci. U.S.A.* **100**, 2065–2069 (2003).
32. A. G. Siapas, M. A. Wilson, Coordinated interactions between hippocampal ripples and cortical spindles during slow-wave sleep. *Neuron* **21**, 1123–1128 (1998).
33. J. N. Gelinas, D. Khodagholy, T. Thesen, O. Devinsky, G. Buzsáki, Interictal epileptiform discharges induce hippocampal-cortical coupling in temporal lobe epilepsy. *Nat. Med.* **22**, 641–648 (2016).
34. D. Dupret, J. O'Neill, B. Pleydell-Bouverie, J. Csicsvari, The reorganization and reactivation of hippocampal maps predict spatial memory performance. *Nat. Neurosci.* **13**, 995–1002 (2010).
35. M. W. Brown, E. C. Warburton, J. P. Aggleton, Recognition memory: Material, processes, and substrates. *Hippocampus* **20**, 1228–1244 (2010).
36. H. P. Davis, L. R. Squire, Protein synthesis and memory: A review. *Psychol. Bull.* **96**, 518–559 (1984).
37. Y. Dudai, Consolidation: Fragility on the road to the engram. *Neuron* **17**, 367–370 (1996).
38. M. E. Judge, D. Quartermain, Characteristics of retrograde amnesia following reactivation of memory in mice. *Physiol. Behav.* **28**, 585–590 (1982).
39. K. Nader, G. E. Schafe, J. E. le Doux, Fear memories require protein synthesis in the amygdala for reconsolidation after retrieval. *Nature* **406**, 722–726 (2000).
40. J. R. Misanin, R. R. Miller, D. J. Lewis, Retrograde amnesia produced by electroconvulsive shock after reactivation of a consolidated memory trace. *Science* **160**, 554–555 (1968).
41. L. Nyberg *et al.*, General and specific brain regions involved in encoding and retrieval of events: What, where, and when. *Proc. Natl. Acad. Sci. U.S.A.* **93**, 11280–11285 (1996).
42. P. J. Hernandez, K. Sadeghian, A. E. Kelley, Early consolidation of instrumental learning requires protein synthesis in the nucleus accumbens. *Nat. Neurosci.* **5**, 1327–1331 (2002).
43. S. J. Cohen *et al.*, The rodent hippocampus is essential for nonspatial object memory. *Curr. Biol.* **23**, 1685–1690 (2013).
44. G. Riedel *et al.*, Reversible neural inactivation reveals hippocampal participation in several memory processes. *Nat. Neurosci.* **2**, 898–905 (1999).
45. P. Piterkin, E. Cole, M. P. Cossette, S. Gaskin, D. G. Mumby, A limited role for the hippocampus in the modulation of novel-object preference by contextual cues. *Learn. Mem.* **15**, 785–791 (2008).
46. S. Tonegawa, M. D. Morrissey, T. Kitamura, The role of engram cells in the systems consolidation of memory. *Nat. Rev. Neurosci.* **19**, 485–498 (2018).
47. I. Izquierdo, J. H. Medina, Memory formation: The sequence of biochemical events in the hippocampus and its connection to activity in other brain structures. *Neurobiol. Learn. Mem.* **68**, 285–316 (1997).
48. S. Gais, M. Mölle, K. Helms, J. Born, Learning-dependent increases in sleep spindle density. *J. Neurosci.* **22**, 6830–6834 (2002).
49. O. Eschenko, M. Mölle, J. Born, S. J. Sara, Elevated sleep spindle density after learning or after retrieval in rats. *J. Neurosci.* **26**, 12914–12920 (2006).
50. G. Girardeau, A. Cei, M. Zugaro, Learning-induced plasticity regulates hippocampal sharp wave-ripple drive. *J. Neurosci.* **34**, 5176–5183 (2014).
51. O. Eschenko, W. Ramadan, M. Mölle, J. Born, S. J. Sara, Sustained increase in hippocampal sharp-wave ripple activity during slow-wave sleep after learning. *Learn. Mem.* **15**, 222–228 (2008).
52. Y. Norman, Hippocampal sharp-wave ripples linked to visual episodic recollection in humans. *Science (1979)* **365**, eaax1030 (2019).
53. E. Stark, M. Abeles, Unbiased estimation of precise temporal correlations between spike trains. *J. Neurosci. Methods* **179**, 90–100 (2009).
54. K. P. Mainali, E. Slud, M. C. Singer, W. F. Fagan "A better index for analysis of co-occurrence and similarity. *Sci Adv* **8**, eabj9204 (2022).
55. L. A. Johnson, D. R. Euston, M. Tatsuno, B. L. McNaughton, Stored-trace reactivation in rat prefrontal cortex is correlated with down-to-up state fluctuation density. *J. Neurosci.* **30**, 2650–2661 (2010).
56. C. W. Dickey *et al.*, Travelling spindles create necessary conditions for spike-timing-dependent plasticity in humans. *Nat. Commun.* **12**, 1027 (2021).
57. G. Buzsáki, Hippocampal sharp wave-ripple: A cognitive biomarker for episodic memory and planning. *Hippocampus* **25**, 1073–1188 (2015).
58. E. Cole, A. Simundic, F. P. Mossa, D. G. Mumby, Assessing object-recognition memory in rats: Pitfalls of the existent tasks and the advantages of a new test. *Learn. Behav.* **47**, 141–155 (2019).
59. Y. Novitskaya, S. J. Sara, N. K. Logothetis, O. Eschenko, Ripple-triggered stimulation of the locus coeruleus during post-learning sleep disrupts ripple/spindle coupling and impairs memory consolidation. *Learn. Mem.* **23**, 238–248 (2016).
60. T. Luft, G. S. Pereira, M. Cammarota, I. Izquierdo, Different time course for the memory facilitating effect of bicuculline in hippocampus, entorhinal cortex, and posterior parietal cortex of rats. *Neurobiol. Learn. Mem.* **82**, 52–56 (2004).
61. P. Ardenghi *et al.*, Late and prolonged post-training memory modulation in entorhinal and parietal cortex by drugs acting on the cAMP/protein kinase A signalling pathway. *Behav. Pharmacol.* **8**, 745–751 (1997).
62. J. I. Rossato *et al.*, Retrograde amnesia induced by drugs acting on different molecular systems. *Behav. Neurosci.* **118**, 563–568 (2004).
63. O. Hardt, K. Nader, L. Nadel, Decay happens: The role of active forgetting in memory. *Trends Cogn. Sci.* **17**, 111–120 (2013).
64. R. K. Pitman *et al.*, Biological studies of post-traumatic stress disorder. *Nat. Rev. Neurosci.* **13**, 769–787 (2012).
65. D. Khodagholy *et al.*, NeuroGrid: Recording action potentials from the surface of the brain. *Nat. Neurosci.* **18**, 310–315 (2015).
66. P. Jastrzebska-Perfect *et al.*, Mixed-conducting particulate composites for soft electronics. *Sci. Adv.* **6**, eaaz6767 (2020).